Journal of Nuclear Materials 162–164 (1989) 562–567
North-Holland, Amsterdam

EDGE DENSITY PROFILE STUDIES IN THE CASTOR TOKAMAK USING A THERMAL LITHIUM BEAM

K. GUENTHER, E. HAYESS, K.H. KREBS, L. WEIXELBAUM and U. WENZEL

Academy of Sciences of the German Democratic Republic, Central Institute of Electron Physics, Hausvogteiplatz 5–7, 1086 Berlin, German Dem. Rep.

J. BADALEC, K. JAKUBKA, J. STOECKEL, M. VALOVIC and F. ZACEK

Czechoslovak Academy of Sciences, Institute of Plasma Physics, Pod vodarenskou vezi 4, CS-18069 Praha 8, Czechoslovakia

Key words: LHCD, SOL structure, fluctuations, Li-beam diagnostics

The plasma edge of the CASTOR tokamak was investigated using a thermal lithium beam and electrical probes. The density profiles in the scrape-off layer (SOL) obtained by means of the lithium beam technique clearly reflect the particular limiter configuration and allow the evaluation in terms of $D_\perp$. These profiles are in good agreement with simultaneous Langmuir probe measurements at different radii. In discharges with additional lower hybrid current drive (OH/LHCD) steeper profiles are obtained, which indicates a reduced radial particle transport. This is supported by the evaluation of fluctuation measurements (density and poloidal electric field) in terms of the turbulent radial particle flux, and by a reduced temporal decay of the line-averaged density during RF. Thus, in effect LHCD improves the particle confinement.

1. Introduction

When LHCD was applied to quasi-stationary ohmic discharges, a tendency of density rise during RF was observed in different tokamaks [1–3]. Detailed studies showed that during LHCD the particle confinement was improved [4]. Moreover, several measurements have shown that the outward particle flux due to the turbulent density and potential fluctuations via the associated $\boldsymbol{E}\times\boldsymbol{B}$ drift could be responsible for the observed anomalous diffusion at the plasma edge in ohmic discharges [5–7].

In order to study the connection of global confinement and fluctuation-induced transport the CASTOR edge plasma was investigated for both OH and LHCD discharges, using two diagnostic techniques simultaneously: density and fluctuation measurements by Langmuir probes, density profile recording by injection of a thermal lithium beam.

Observation of the visible light emitted by excited lithium atoms due to electron collision allows the determination if the electron density profile as an absolute quantity of the light emission is recorded up to the total absorption (ionization) of the beam [8]. For this purpose a beam with an energy in the range of 0.1 to 10 eV has been employed as already reported elsewhere (thermal beam [9], laser ablated beam [10]). Moreover, to allow for the velocity distribution of the atoms, it is necessary to extend the observation region up to the onset of the signal at $x = x_0$ (entrance of the beam into the plasma where $n_e \simeq 0$). The local electron density $n_e(x)$ can be evaluated from the recorded light intensity profile $s(x)$ by

$$n_e(x) = \frac{s(x)v_0}{\xi_i \int_x^\infty \mathrm{d}x' s(x')} F(H),$$

$$H = \frac{\int_x^\infty \mathrm{d}x' s(x')}{\int_{x_0}^\infty \mathrm{d}x' s(x')}, \qquad (1)$$

where v_0 is the mean velocity at the beam entrance, ξ_i the rate coefficient of ionization, and $F(H)$ a function which depends on the initial velocity distribution. For an atomic beam with Maxwellian velocity distribution as in the case of our thermal source $F(H)$ is shown in fig. 1. Two prerequisites have to be fulfilled for the application of eq. (1): (1) the ratio of the rate coefficients for ionization and excitation is independent of

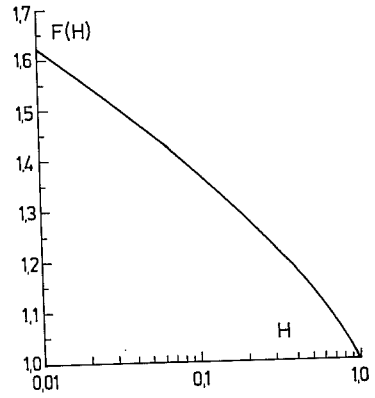

Fig. 1. Correction function $F(H)$ for a Maxwellian velocity distribution.

the radial distance r, i.e. of T_e, and (2) the electron density is sufficiently low so that ionization from excited levels is negligible.

2. Experiment

The parameters of the CASTOR tokamak and the discharge parameters are:

major radius	$R_0 = 0.4$ m,
liner radius	$a = 0.1$ m,
toroidal magnetic field	$B_t = 1.3$ T,
plasma current	$I_p = 12$ kA,
line-averaged density	$n_e = 5 \times 10^{18}/\mathrm{m}^3$,
edge temperature	T_e(SOL) = 20 eV (measured by Langmuir probe),
working gas	hydrogen
limiter configuration	– fixed aperture limiter at $r = 85$ mm – one or two movable sector limiters at $r = 74$ mm.

The experimental set-up is shown in fig. 2. The lithium beam was injected into the plasma nearly radially from an oven heated to about 950 K. A collimator tube led the beam up to the liner radius (beam sectional area 10×10 mm) and collision losses were reduced by setting a differential pump in the beam path. In this way a sufficiently high lithium density was achieved in a distance of about 0.5 m from the relative small oven (volume 2 cm^3, effusion area 0.28 cm^2). The radial interval from $r = 30$ mm to $r = 100$ mm was imaged on a linear CCD array, and the resonance radiation at 671 nm was observed through an interference filter of fwhm = 4 nm. Lithium beam measurements were accompanied by several Langmuir probe measurements. By means of a fixed triple probe at $r = 85$ (on the top of the torus) the fluctuations of density $\tilde{n}_e$ and mm poloidal electrical field $\tilde{E}_p$ and (by cross correlation of $\tilde{n}_e$ and $\tilde{E}_p$) the turbulent radial flux Γ_{turb} were measured. A

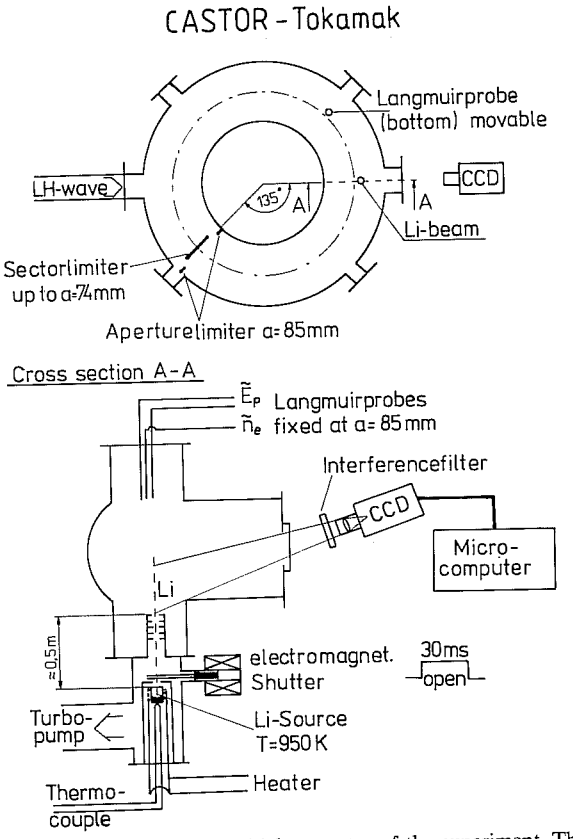

Fig. 2. Toroidal and poloidal geometry of the experiment. The sector limiters are located at top and bottom of the torus.

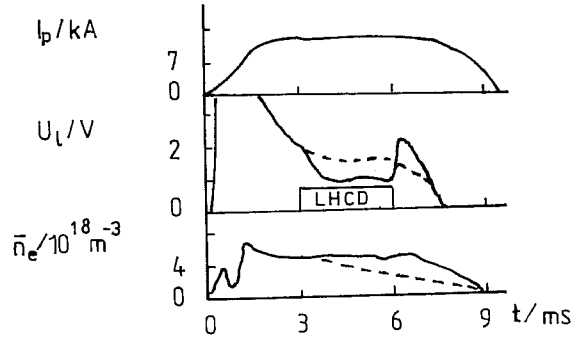

Fig. 3. Plasma current, loop voltage and line-averaged density of OH/LHCD (full line) and OH (dotted line) discharges.

single probe (diameter 0.6 mm), movable from shot to shot, at the same poloidal position as the lithium beam (at bottom) gave comparable values of the density in dependence on the minor radius.

In the non-induced current drive experiment RF power ($f = 1.25$ GHz, $P = 40$ kW) was launched into the plasma via a grill consisting of three parallel waveguides. A characterization of these discharges is given in fig. 3. No additional gas feed was applied to hold $\bar{n}_e$ constant. When part of the current is driven by the LH waves as indicated by the drop of the loop voltage the density decay stops until the end of the RF pulse. Additional experiments have shown that the RF power launched into a discharge in the gas puffing regime ($\bar{n}_e$ constant in ohmic discharges) causes a rise of the line-averaged density. This behaviour is a first indication of improved particle confinement. For details concerning LHCD on the CASTOR tokamak see [11,12].

3. Results and discussion

The signal profiles depend on the moment of observation during the discharge, the limiter configuration and the plasma parameters. Fig. 4 shows signal profiles at different moments during the discharge. They reflect the temporal behaviour of the plasma parameters (decreasing line-averaged density, change of the profile due to LHCD from 3–6 ms) as well as a displacement of the plasma column (upward due to magnetic stray fields and inward due to the falling pressure). In the following only the profiles during 3–6 ms (second scan of the CCD camera) corrected for the plasma displacement according to the data from the magnetic diagnostics given in [12] will be considered. The density profiles derived will be given in terms of r, the minor radius of the plasma column.

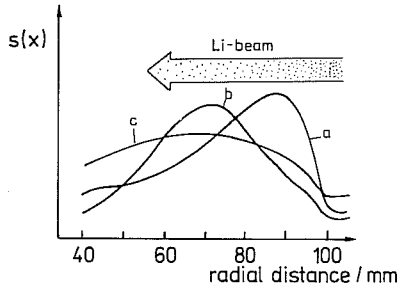

Fig. 4. Intensity profiles of the lithium radiation in an OH/LHCD discharge (integration time 3 ms); (a) 0–3 ms; (b) 3–6 ms; (c) 6–9 ms.

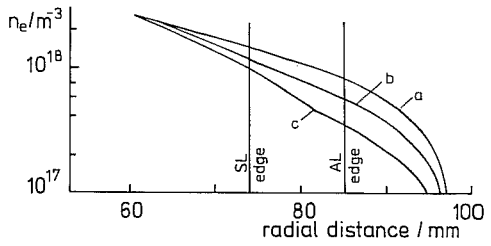

Fig. 5. Electron density profiles of OH/LHCD discharges with different limiter configurations: (a) aperture limiter only; (b) one additional sector limiter; (c) two additional sector limiters.

3.1. Edge density profiles for different limiter configurations in discharges with current drive

The density profiles shown in fig. 5 have been obtained from discharges with similar line-averaged densities. For clearness only, curve (a) has been multiplied by a factor of 1.35. Regarding the slope, the curves (b) and (c) compared with (a) clearly exhibit the influence of the sector limiters. The density profiles obtained with either one of the two sector limiters (at top or bottom of the torus) are practically indistinguishable (curve (b)), which is surprising at first glance, considering that some non-uniformity in the structure of the SOL should generally be expected due to the symmetry-breaking effect of sector limiters [13,14]. However, the safety factor q reaches a value of 8 just in the sector limiter shadow (at $r = 77$ mm exactly), and the poloidal extension of a sector limiter is only a little smaller than 45°, which leads to the particular situation that the entire SOL consists of almost only a single flux tube bundle whose connection length $L_\parallel$ amounts to 8 circumferences of the torus ($360°/45° = 8$). The same is true if both sector limiters are active (4 circumferences). Therefore, the simple 1D description of the SOL, including the aperture limiter shadow ($L_\parallel = 2\pi R_0$) too, can be applied:

$$\frac{\mathrm{d}}{\mathrm{d}r} D_\perp \frac{\mathrm{d}n_e}{\mathrm{d}r} = \frac{\Delta\vartheta/360°}{\pi R_0} f c_s n_e, \qquad (2)$$

where $f < 1$ is the longitudinal profile factor and $\Delta\vartheta$ the poloidal extension of the limiters corresponding to the radius r. In the following, $f = 0.69$ is used according to [14,15].

The curves in fig. 5 do not allow a simple evaluation in terms of decay lengths λ, since the radial extension of the sector limiter shadow is equal to or even less than an e-folding length of density decay. Instead, one has to rest on a complete solution of the second-order eq. (2) which is easy to obtain by setting $D_\perp$ constant. This

approach, however, fails: there is no constant $D_\perp$ that can reproduce the experimental profiles. The strict analysis by solving eq. (2) results in

$$D_\perp(r) = \frac{f}{\pi R_0} \frac{\text{const} + \int_r^{r_0} \mathrm{d}r (\Delta\vartheta/360°) c_s n_e}{-\mathrm{d}n_e/\mathrm{d}r}, \quad (3)$$

where $r_0 \simeq 95$ mm is the radius up to which $n_e(r)$ has been reliably measured. However, an unambiguous result of this approach would require the knowledge of a boundary value $D_\perp(r_0)$.

Nevertheless, it follows from eq. (3) with the experimental $n_e(r)$ inserted that the physically reasonable solutions show a flat maximum of $D_\perp$ in the sector limiter shadow. This value is easy to obtain because of the fortuitous fact that the density profiles (b) and (c) (in contrast to (a)) exhibit an exponential behaviour just in that range ($r = 74$–85 mm), where $n_e = n_0 \exp(-r/\lambda)$ is a solution of eq. (2) for $D_\perp$ = constant with $\lambda = (\pi R_0 D_\perp / f c_s(\Delta\vartheta/360°))^{1/2}$. From the curves (b) and (c) we obtain $\lambda = 15.5$ mm and $\lambda = 10.7$ mm, respectively. Thus, the ratio is in fact close to the expected value $\sqrt{2}$ ($\Delta\vartheta = 40°$ and $80°$, respectively), which supports this analysis, and leads to the common diffusion coefficient

$$D_\perp = 0.89 \text{ m}^2/\text{s} \quad (4)$$

with $c_s = (2T_e/m_i)^{1/2}$. This value is near to the Bohm diffusion coefficient (0.96 m^2/s).

3.2. Comparison between Langmuir and lithium beam measurements

The simultaneous measurement of electron density by Langmuir probe and thermal lithium beam allows a cross-check of both methods. A probe produces its own presheath region highly elongated along the magnetic field. In this region ions are accelerated towards the sheath. The extension of this "collection region" results from the condition that cross-field diffusion must be able to balance the parallel collected flow and is a few times $c_s d^2/D_\perp$, where d is the probe diameter. At the sheath edge the density is reduced compared with n_∞, the unperturbed density which is to be determined. According to Hutchinson's one-dimensional fluid theory approach [16] the ion saturation current density is given by $0.35 e n_\infty c_s$, where the reduction factor 0.35 applies to a surrounding plasma at rest, otherwise the corresponding average (upstream and downstream) is only insignificantly larger, at least for the major part of the SOL (moderate flow velocity in sufficient distance from the limiter surface).

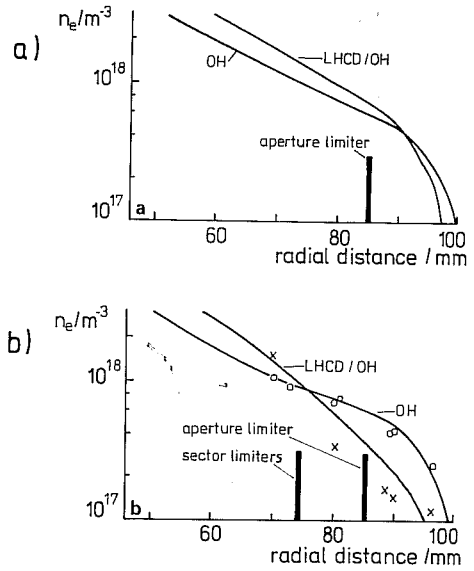

Fig. 6. Density profiles of OH and OH/LHCD discharges (RF: 3–6 ms): (a) aperture limiter only; (b) aperture limiter and both sector limiters. Results obtained from Langmuir probe are indicated by symbols.

In Fig. 6(b) the results of both methods are compared. The collection region of our small probe is very short (25 mm) according to the above expression, using the parameters given in the text. So Hutchinson's formula is applicable. The agreement of the obtained density profiles is good, especially for ohmic discharges.

3.3. Improved particle confinement during LHCD

In fig. 6 the edge density profiles of OH and OH/LHCD discharged are compared for two different limiter configurations. The substantial difference in the slope shows that LHCD reduces the radial transport of particles in terms of $D_\perp$, which turns out to be Bohm-like (cf. eq. (4)).

Ohmic discharges are characterized by a flatter gradient, which implies an increased $D_\perp$ provided that the particle flux is not reduced. From a comparison of the temporal dependence of the line-averaged densities (see fig. 3) it can be concluded that the efflux in ohmic discharges is even larger. An alternative explanation for the continuous temporal decay by assuming a smaller influx of neutrals can be ruled out, since according to earlier measurements a nearly unchanged influx of impurities and neutral hydrogen during LHCD has been observed [17].

Note that the increased $D_\perp$ leads to a decreased scraping-off of particles by the small sector limiters which explains the almost coincident OH profiles in fig. 6(a) and (b). This leads to a nearly constant dn_e/dr within the sector limiter shadow and makes it impossible to derive $D_\perp$ from the measured density profile, as done in section 3.1.

These conclusions are borne out by the results of the fluctuation measurements. Fig. 7 shows that during the RF pulse the fluctuations at $r = 85$ mm go down, which results in a drastic reduction of the turbulent radial particle flux (fig. 7d) as estimated from $\Gamma_{turb} = C\tilde{n}_e\tilde{E}_p/B_t$ ($\boldsymbol{E}\times\boldsymbol{B}$ drift), where C is the cross correlation factor of $\tilde{n}_e$ and $\tilde{E}_p$. Absolute values of Γ_{turb} combined with dn_e/dr from measured density profiles allow an independent determination of $D_\perp$, if Γ_{turb} is taken for the total flux of particles. However, our LHCD results are not well suited for that purpose because the RF power was launched at different time intervals in

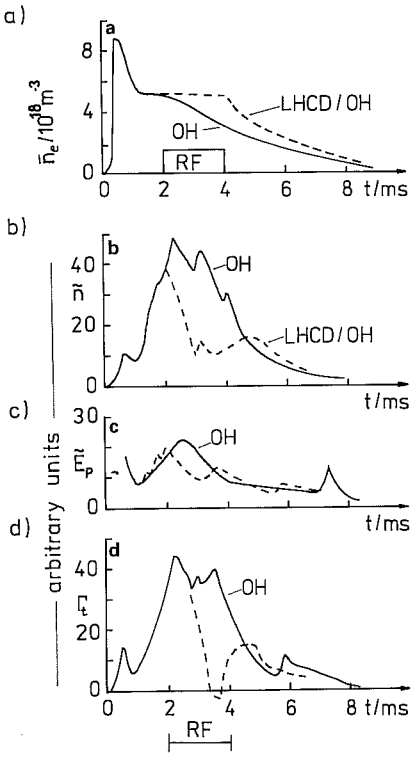

Fig. 7. Line-averaged density (a), density (b) and poloidal electric field (c) fluctuations, turbulent radial particle flux (d) for OH (full line) and OH/LHCD (dotted line) discharges determined with the triple probe at $r = 85$ mm. Both sector limiters withdrawn.

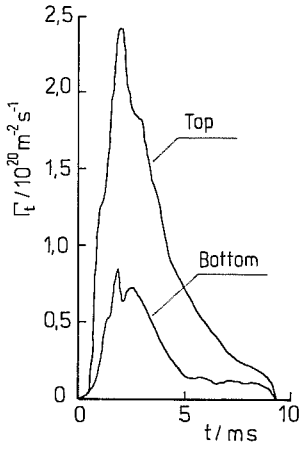

Fig. 8. Up/down asymmetry of the turbulent radial flux in an OH discharge at $r = 85$ mm. Both sector limiters withdrawn.

both experiments (see figs. 3 and 7). Moreover, pure OH experiments with the triple probe installed at the bottom of the torus revealed the existence of a considerable up/down asymmetry of Γ_{turb} as shown in fig. 8.

Therefore, let us take these OH results and the corresponding density profile in fig. 6(a) ($-dn_e/dr = 2.7\times10^{19}/m^4$ at $r = 85$ mm) to derive $D_\perp$ from the temporal and up/down average of Γ_{turb} ($q \approx 8$ should ensure a sufficient poloidal mix). The averaged value of Γ_{turb} between 3 and 6 ms can be estimated from fig. 8 to be $6\times10^{19}/m^2$ s, which then yields $D_\perp = 2.2$ m^2/s at $r = 85$ mm. This result demonstrates the consistence of the different experimental approaches.

4. Conclusions

The thermal lithium beam technique has proved to be a reliable method to determine electron density profiles in the edge plasma of a tokamak. This is confirmed by the excellent reproducibility and the good agreement with Langmuir probe measurements. By a differential local analysis of the density profiles with respect to the balance of particle flux divergence and sink strength in the SOL (dependent on the limiter configuration) the diffusion coefficient $D_\perp = 0.89$ m^2/s for OH/LHCD discharges was derived. It turns out to be Bohm-like. However ohmic discharges are characterized by a much higher $D_\perp$. This deterioration of confinement is a direct consequence of the enhanced turbulent flux as detected by measurements of the fluctuations of both plasma density and poloidal electric field at the separatrix . $D_\perp$ derived from the turbu-

lent flux in ohmic discharges is roughly 2.2 m^2/s. Two conclusions can be drawn: (1) LHCD improves the particle confinement. (2) The $\boldsymbol{E} \times \boldsymbol{B}$-driven turbulent flux is likely to be at least the preponderant component of the anomalous radial diffusion of particles.

Acknowledgements

This work was supported by the IAEA Contract No. 4552/R1/RB. The authors are also grateful to J. Lingertat for continuous stimulation and encouragement.

References

[1] S.C. Luckhardt et al., Phys. Rev. Lett. 48 (1982) 152.
[2] V.V. Alikaev et al., Fisika Plasmi 11 (1985) 53.
[3] J. Badalec, Proc. 14th Czeochoslovak Seminar on Plasma Physics and Technology, Liblice, 1987.
[4] S.C. Luckhardt et al., Phys. Fluids 29 (1986) 1985.
[5] S.J. Zweben and R.W. Gould, Nucl. Fusion 25 (1985) 171.
[6] V.P. Budaev and R.S. Ivanov, in: Proc. 12th European Conf. on Plasma Physics, Budapest, 1985, paper AP FR 024, Vol. 1, p. 303.
[7] A.J. Wooton et al., Oak Ridge Report ORNL-TM-9305 (1986).
[8] U. Hintz and P. Bogen, J. Nucl. Mater. 128 & 129 (1984) 229.
[9] U. Samm et al., J. Nucl. Mater. 145–147 (1987) 206.
[10] A. Pospieszczyk and G.G. Ross, in: Proc. 14th European Conf. on Controlled Fusion and Plasma Physics, Madrid, 1987, paper CP 1280, Vol. 3, p. 1280.
[11] J. Badalec et al., Fisika Plasmi 14 (1988) 395.
[12] M. Valovic, Czech. J. Phys. B38 (1988) 55.
[13] K.F. Alexander et al., in: Proc. 11th Int. Conf. on Plasma Physics and Nuclear Fusion Research, Kyoto, 1986, paper IAEA-CN-47/a-IV-5, Vol. 1, p. 237.
[14] J. Lingertat et al., Plasma Phys. Contr. Fusion 29 (1987) 1365.
[15] K. Guenther, Contrib. Plasma Phys. 28 (1988) 365.
[16] I.H. Hutchinson, Phys. Fluids 30 (1987) 3777.
[17] J. Stoeckel et al., IPPCZ Report No. 279 (1988).